Effect of a Heterogeneous Network on the Fracture Behavior of Epoxy Resins

Shundo, Atsuomi
Department of Automotive Science, Kyushu University

Aoki, Mika
Center for Polymer Interface and Molecular Adhesion Science, Kyushu University

Wang, Pangpang
Materials Open Lab., Institute of Systems, Information Technologies and Nanotechnologies

Hoshino, Taiki
International Center for Synchrotron Radiation Innovation Smart, Tohoku University

他

出版情報：Macromolecules. 56 (11), pp.3884-3890, 2023-05-30. American Chemical Society (ACS)
バージョン：

Effect of Heterogeneous Network on Fracture Behavior of Epoxy Resins

Atsuomi Shundo[a]*, Mika Aoki[b], Pangpang Wang[c], Taiki Hoshino[d,e], Satoru Yamamoto[b], Sunao Yamada[c] and Keiji Tanaka[a,b,f]*

[a] *Department of Automotive Science, Kyushu University, Fukuoka 819-0395, Japan*

[b] *Center for Polymer Interface and Molecular Adhesion Science, Kyushu University, Fukuoka 819-0395, Japan*

[c] *Materials Open Lab., Institute of Systems, Information Technologies and Nanotechnologies, Fukuoka 814-0001, Japan*

[d] *International Center for Synchrotron Radiation Innovation Smart, Tohoku University, Sendai 980-8577, Japan*

[e] *RIKEN SPring-8 Center, Hyogo 679-5148, Japan*

[f] *Department of Applied Chemistry, Kyushu University, Fukuoka 819-0395, Japan*

*CORRESPONDING AUTHORS:

Tel: +81-92-802-2880 (A.S.) & +81-92-802-2878 (K.T.)

E-mail: a-shundo@cstf.kyushu-u.ac.jp (A.S.) & k-tanaka@cstf.kyushu-u.ac.jp (K.T.)

For Table of Contents used only

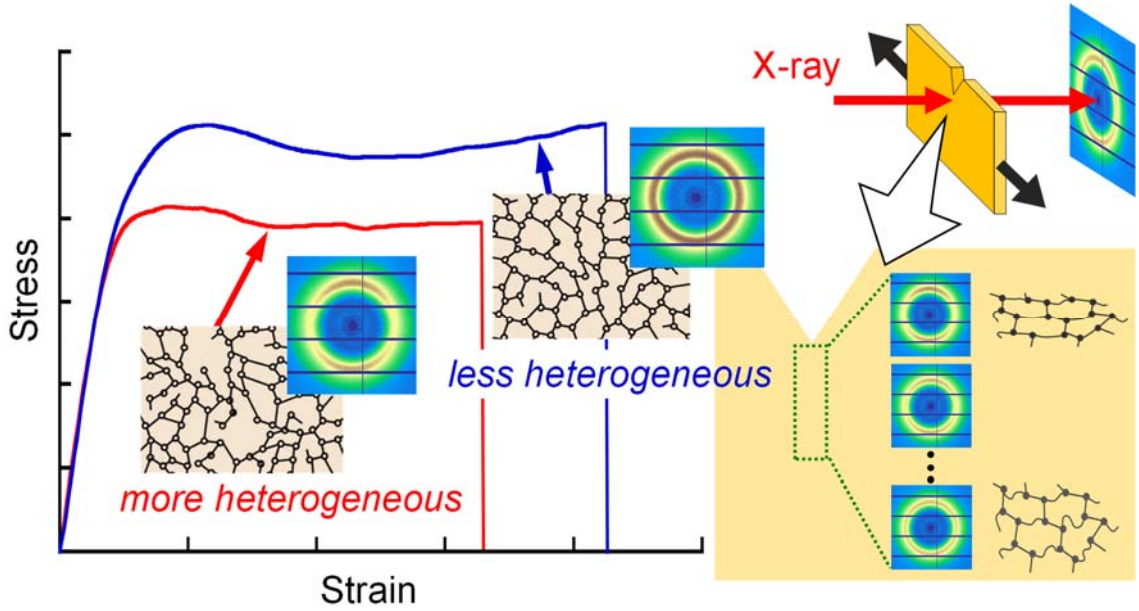

ABSTRACT

Epoxy resins, which possess a three-dimensional network obtained by a curing reaction between epoxy and amine compounds, are in a glassy state at room temperature. They are therefore generally brittle and exhibit rather poor resistance to crack propagation, which is one of the greatest drawbacks for their practical application. To solve this problem, a better understanding of their fracture behavior, which is related to long-term durability, has been strongly desired. We herein report on how the extent of network heterogeneity affects the fracture behavior of epoxy resins. Three types of epoxy resins were obtained under different curing conditions, which generated different extents of heterogeneity. The fracture behavior of the three epoxy resins was examined by *in-situ* scanning electron microscopy in conjunction with microbeam X-ray scattering experiments. When the epoxy resin in which a notch was pre-introduced was stretched under a small strain, the internal network structure was deformed and the extent was more significant with increasing heterogeneity. As further stretching was applied, a crack was propagated from the notch. This occurred more easily with increasing heterogeneity. That is, the toughness of the epoxy resins decreased with increasing network heterogeneity. The knowledge here obtained will be useful for understanding and controlling the toughness of epoxy resins.

1. INTRODUCTION

Epoxy resins, obtained by the curing reaction of epoxies with amine compounds, are one of the important classes of thermosets and have an internal three-dimensional network. They are used across a wide range of industrial fields in materials such as adhesives,[1–3] coatings,[4,5] encapsulants[6,7] and composite matrices,[8,9] thanks to their excellent mechanical properties, good corrosion resistance and electrical insulation properties. However, they are generally brittle and exhibit poor resistance to crack propagation because they are in a glassy state at room temperature.[10,11] This is one of the biggest drawbacks for their use as a structural material and adhesive.[3,12] To solve this problem, there is a strong demand for a better understanding of the fracture behavior, which is directly linked to long-term durability.

In general, the fracture behavior of polymer materials including epoxy resins involves craze generation (crazing), void formation, shear yielding and/or plastic deformation.[13–18] These events at cracks and/or other stress-induced defects are responsible for energy dissipation during the fracture process and thus play a crucial role in the control of fracture toughness.[19] Thus, great efforts have been made to examine the crazing and/or void formation associated with the cross-linking density of the network in epoxy resins.[20–22] Studies have shown that, while no crazing is observed for fully-cured resins, it is observed for partially-cured ones or those with a relatively low cross-linking density.[22,23] Given that crazing suppresses crack propagation and thus improves the fracture toughness, this toughness should increase with decreasing cross-linking density. Although this has been confirmed by the findings of some studies, there have been reported exceptions.[24,25] Thus, we are still some way from understanding how the network affects the fracture behavior of epoxy resins.

It has recently been reported that actively-reacted domains surrounded by scarcely-reacted regions were formed even at the initial stage of the curing process of an epoxy resin and these grew in size as the curing process proceeded.[26–28] The resultant epoxy resin was spatially

heterogeneous in terms of the network structure, and the extent of the heterogeneity was dependent on the curing temperature, which altered how the network was formed.[27] Interestingly, once the epoxy resin was immersed in a good solvent, it was partially swollen and then macroscopically fractured. The immersion time, at which the macroscopic fracture occurred, decreased as the extent of the heterogeneity increased.[27] Considering the results of the solvent-crack test, it is supposed that the fracture behavior of epoxy resins depends on the extent of the heterogeneity. Nevertheless, there are few published reports on this issue.

We herein report on how the extent of the network heterogeneity affects the fracture behavior of epoxy resins. Three types of epoxy resins were prepared under different curing conditions, which generated different extents of heterogeneity. Fracture strain and toughness of the three epoxy resins were examined by tensile tests. The crack propagation from a notch, which was pre-introduced to the epoxy resin, was observed by *in-situ* scanning electron microscopy (SEM). The crazing and/or void formation around the crack was examined by ultra-small-angle X-ray scattering (USAXS) measurement with an X-ray microbeam.[29–31] Finally, microbeam wide-angle X-ray scattering (WAXS) provided information on the local deformation of the network, which could be associated with the crack length and the toughness of the epoxy resins.

2. EXPERIMENTAL

2.1. Materials and preparation of epoxy resins. Panel (a) of Figure 1 shows the chemical structure of hydrogenated diglycidyl ether of bisphenol-A (HDGEBA) and 1,4-cyclohexanebis(methylamine) (CBMA), respectively, purchased from New Japan Chemical Co., Ltd. and Tokyo Chemical Industry Co., Ltd. HDGEBA and CBMA were mixed at a stoichiometric molar ratio of 2:1. The mixture, which was placed in a silicon mold, was cured via three steps. The first step, named pre-curing, was performed at 296 K for 24 h, 323 K for

12 h, or 353 K for 3 h for three individual mixtures. The three different temperatures were employed to alter the extent of the heterogeneity in the network.[27] The holding time at each pre-curing temperature was chosen as a length which for the reaction conversion remained unchanged, as suggested by Fourier-transform infrared (FT-IR) spectroscopy.[26,27] The second step, named middle-curing, was performed at 373 K for 1 h. Since the middle-curing temperature of 373 K was higher than the glass transition temperature (T_g) of the system, the period of 1 h should be sufficient for an apparent completion of the reaction.[27] The third step, named post-curing, was conducted at 393 K for 6, 3, or 2 h after the middle-curing. During the post-curing at 393 K, the cross-linking density increased over the time. The discrepancy in the post-curing time was for unifying their cross-linking density.[27] The resins obtained after the three steps are hereafter denoted as ER296, ER323, and ER353, where the latter number simply corresponds to the pre-curing temperature.

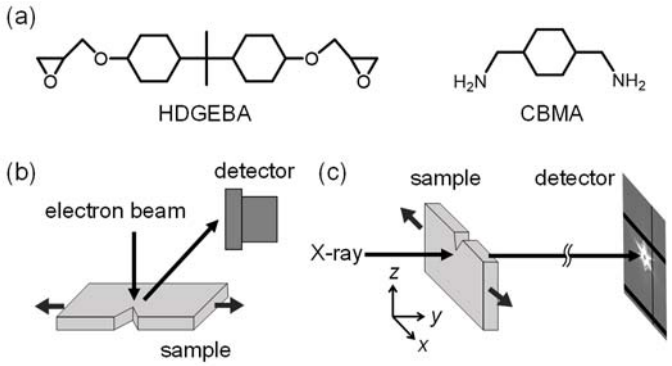

Figure 1. Chemical structure of (a) HDGEBA and CBMA. Schematic illustrations of experimental setups for (b) *in-situ* SEM observation and (c) microbeam USAXS and WAXS measurements.

2.2. Characterizations. The cross-linking density (ν) of the cured epoxy resins was estimated based on the swelling ratio in tetrahydrofuran (THF), which is a good solvent, via the Flory–Rehner equation.[27,32] The mass density (ρ) was examined by a gas pycnometer (ULTRAPYC 1200e, Quantachrome Instruments Inc.) with a helium probe. The target pressure

of the helium gas was set at 117 kPa and the measurement was repeated 100 times to take an average. The T_g was examined by differential scanning calorimetry (DSC) (DSC6220, SII Nanotechnology Inc.). Samples were heated up to 473 K at a rate of 10 K·min^{-1} under a dry nitrogen purge and then cooled down to 273 K. The first heating scan was used for the determination of T_g. The mechanical properties of the epoxy resins were characterized by tensile testing using a TENSILON RTF-1310 (A&D Co., Ltd.). Specimens for the tensile test were prepared by placing the epoxy−amine mixture into a dumbbell-shaped mold made of a silicone rubber and an aluminum substrate, followed by the three-step curing processes. The shape of the specimens so obtained conformed to the Japanese Industrial Standards (JIS), K6251-7, which had a gauge length of 12 mm and a width of 2 mm. The tensile test was conducted at room temperature with a crosshead speed of 10 mm·min^{-1}. The strain was determined based on a crosshead displacement.

2.3. Scanning electron microscopy. A dumbbell-shaped specimen with a triangular notch was used for the SEM observation (see Figure S1 in the Supporting Information). The HDGEBA−CBMA mixture was placed into the mold, which had the target shape, and then cured under the same conditions as described in section 2.1. The thickness of the specimens was ca. 0.5 mm. Prior to the SEM observation, the specimen was coated with a 5 nm-thick layer of platinum by an ion-sputtering device MSP-20-UM (Vacuum Device Inc.).

The surface morphology of the epoxy resins, which were stretched at a strain of 0 and 0.05, was observed by a Helios NanoLab 600i (Thermo Fisher Scientific). The stretching was achieved using a tensile test stage TS-1500-II (TSL Solutions Co., Ltd.) with a crosshead speed of 0.025 mm·min^{-1}. Working distance, accelerating voltage and beam current were set at 26 mm, 2 kV and 21 pA, respectively. Panel (b) of Figure 1 shows a schematic illustration of the setup for the SEM observation with the tensile stage.

2.4. Microbeam X-ray scattering measurements. Microbeam USAXS and WAXS

experiments were performed at the BL05XU beamline of SPring-8 (Japan Synchrotron Radiation Research Institute). The wavelength and spot size of the incident X-ray were 0.10 nm and ca. 10 × 10 μm^2, respectively. The sample-to-detector distances for the USAXS and WAXS measurements were ca. 3,800 mm and ca. 250 mm, respectively. The scattered X-rays were recorded using a PILATUS 1M (DECTRIS Ltd.). The dumbbell-shaped specimen with a triangular notch was fixed on a tensile testing device, OZ520 (SENTEC Co., Ltd.) on a sample stage, and then stretched at a strain of 0.05 for USAXS and 0.03 for WAXS. To determine the position of the notch tip, X-ray transmittance was obtained by moving the sample stage (see Figure S2 in the Supporting Information).[14] Then, USAXS or WAXS patterns were acquired by moving the sample stage with an interval distance of 10 μm in the *z*-directions from the notch tip. Panel (c) of Figure 1 shows a schematic illustration of the experimental setup.

3. RESULTS AND DISCUSSION

3.1. Mechanical properties associated with network heterogeneity.

Table 1 summarizes the characterization data for the ν, ρ and T_g values for ER296, ER323, and ER353. The ν and ρ values for all samples were the same. In general, ν and ρ are closely related to the T_g value.[33] Nevertheless, the T_g value was lower in the order of ER353, ER323, and ER296. The network formation during the pre-curing process was dependent on temperature, as suggested by FT-IR spectroscopy, which detected the difference in the generation of the secondary and tertiary amines, in conjunction with coarse-grained molecular dynamics simulation.[27,34] At lower temperatures, homogeneous domains were formed, unreacted substances were incorporated into them, and the network grew. At higher temperatures, the reaction proceeded rapidly before unreacted substances were incorporated into domains, leaving isolated small fragments and nanoscale voids, free spaces, in the network. The resultant network became more heterogeneous, as the pre-curing temperature

increased.[27,34] That is, there were denser and less-dense regions in the network structure. Given that the number density of dangling chains, in which one end attaches to the network and the other is free, increases with increasing network heterogeneity, a decrease in T_g with increasing pre-curing temperature can be understood.[33,35]

Table 1. The ν, ρ and T_g values for ER296, ER323, and ER353.

	$\nu \cdot 10^{-3}$ / mol·m^{-3}	ρ / g·cm^{-3}	T_g / K
ER296	1.59 ± 0.01	1.104 ± 0.008	373 ± 1
ER323	1.60 ± 0.02	1.103 ± 0.007	370 ± 1
ER353	1.59 ± 0.01	1.104 ± 0.006	366 ± 0.3

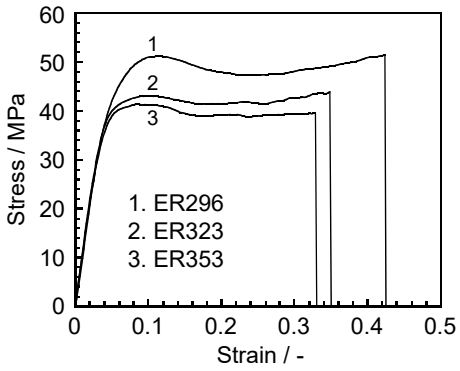

Figure 2. S–S curves for ER296, ER323 and ER353.

Figure 2 shows representative stress-strain (S–S) curves for ER296, ER323, and ER353. Their S−S curves contain initial elasticity and yielding regions before reaching a fracture. Table 2 lists Young's modulus (E), yielding stress (σ_y), fracture strain (ε_f) and fracture energy (G_f) averaged over 10 different specimens of each sample. The G_f value was determined based on the area under the S–S curve and used as an index of the material toughness. The E value for all samples was the same within the range of the experimental error. This seems reasonable because the ν and ρ values for all samples were the same as one another, as shown in Table 1. An important fact is that the σ_y and ε_f, and thereby the G_f, were lower in the order of ER353, ER323, and ER296. Taking into account that the network structure became more heterogeneous with increasing pre-curing temperature,[27] it seems reasonable that as the network became more

heterogeneous, the toughness decreased.

Table 2. Young's modulus (E), yielding stress (σ_y), fracture strain (ε_f), and fracture energy (G_f) for ER296, ER323, and ER353.

sample	E / GPa	σ_y / MPa	ε_f / -	G_f / MJ·m^{-3}
ER296	1.10±0.07	51.1±1.4	0.40±0.07	14.7±3.6
ER323	1.06±0.03	44.1±0.9	0.34±0.06	13.7±2.8
ER353	1.02±0.03	43.2±1.1	0.29±0.06	11.8±1.9

3.2. Stretch-induced crack behavior.

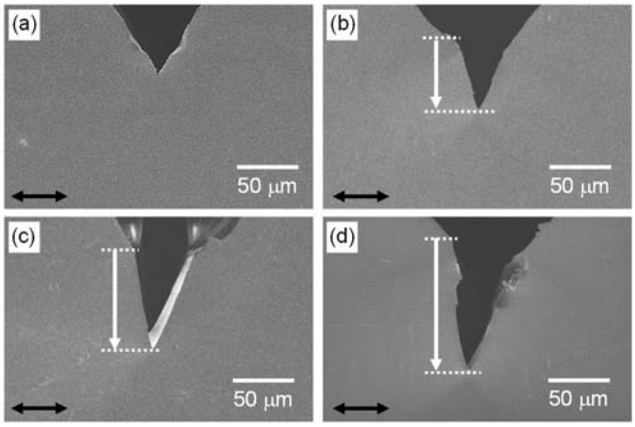

Figure 3. SEM images near a notch tip for (a, b) ER296, (c) ER323 and (d) ER353 at ε of (a) 0 and (b, c, d) 0.05. The white arrows correspond to the crack length and the black double arrows denote the stretching direction.

Prior to the SEM observation, a notch was introduced to a dumbbell-shaped specimen of the epoxy resin. The crack propagation from the notch tip upon the stretching was observed. Once the crack was generated, it continuously propagated but not in a stick-slip manner.[36] Figure 3 shows SEM images of (a, b) ER296, (c) ER323, and (d) ER353 near the notch tip at a strain (ε) of (a) 0 and (b, c and d) 0.05. As shown in panel (a), the notch for a representative sample, ER296, was triangular in shape. For ER296 stretched at ε of 0.05, the crack from the notch tip was clearly observed. While the strain was maintained at 0.05, further propagation of the crack did not occur so the length of the crack remained unchanged. This was also the case for ER323 and ER353. An important fact here is that the crack length was longer in the order

of ER353, ER323, and ER296. This made it clear that the crack grew facilely with an increasing heterogeneity of the network. This is consistent with the result that the ε_f and G_f values were higher in the order of ER296, ER323, and ER353.

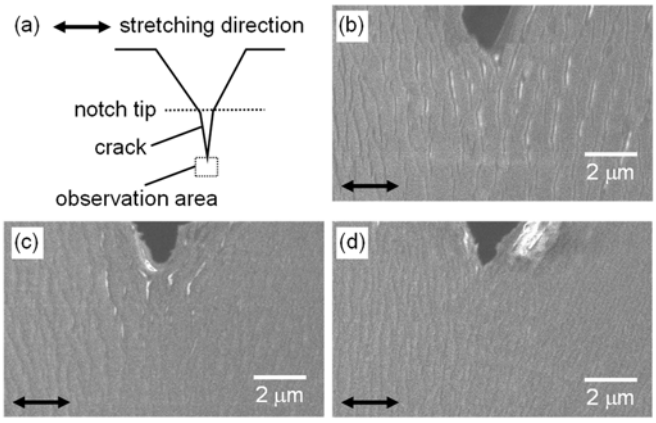

Figure 4. (a) A schematic illustration of an observation area near a crack tip, and SEM images near a crack tip for (b) ER296, (c) ER323 and (d) ER353 at ε of 0.05. The black double arrows denote the stretching direction.

The area near the crack tip was observed at a higher magnification, as illustrated in Figure 4(a). Panels (b, c and d) of Figure 4 show magnified images for (b) ER296, (c) ER323, and (d) ER353. For all samples, a stripe pattern composed of white-colored parts was observed along the direction parallel to the crack propagation, i.e. perpendicular to the stretching direction. The generation of the stripe pattern can be explained as follows.[37] The surface of the epoxy resin was coated with a thin layer of platinum to avoid charge up during the observation. Upon stretching, the underlying epoxy resin was exposed to the surface due to the cracking of the platinum layer so the exposed area became charged, resulting in the appearance of white parts as the striped pattern. Here, it is noteworthy that the periodic distance between adjacent stripes was longer in the order of ER353, ER323, and ER296, as shown in Figure 4. Although the reasons for this finding are not yet clear, it is presumable that the extent of the deformation near the crack tip differs, depending on the extent of the heterogeneity. This issue will be discussed in a later section.

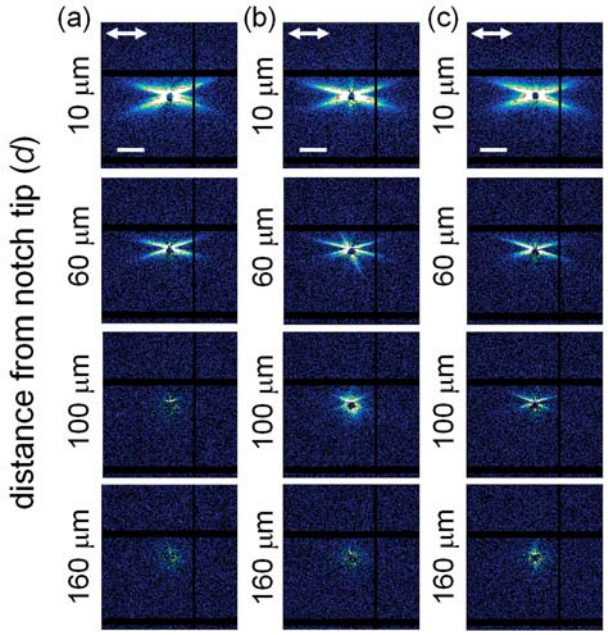

Figure 5. Two-dimensional USAXS patterns at various *d*s for (a) ER296, (b) ER323 and (c) ER353 at ε of 0.05. The white double arrows in the top row denote the stretching direction. Scale bars correspond to 200 nm^{-1}.

In general, stretch-induced cracking for glassy polymers is supposed to be a result of the generation of crazes and/or micro-sized voids.[38,39] To gain access to the formation of the crazes and/or microvoids in the specimen, which cannot be observed by SEM, USAXS measurements with micrometer-sized incident X-ray beams were conducted. The scattered X-ray was acquired at different locations along the direction normal to the notch and crack for each specimen stretched at ε of 0.05. Figure 5 shows representative two-dimensional (2D) USAXS patterns, which were collected at a position (*d*) of 10, 60, 100, and 160 μm away from the notch tip, which was determined in position by the X-ray transmittance measurement (see Figure S2 in the Supporting Information).[14] Each pattern was subtracted by the corresponding one obtained for the upstretched sample to remove the contribution of parasitic scattering. For all samples, an X-shaped pattern was observed at a *d* of 10 μm. This pattern corresponds to the crack, as evidenced by Fourier transform (FT) of SEM images (see Figure S3 in the Supporting Information). The X-shaped pattern was also observed at a $d > 10$ μm. However, the *d* value,

at which the X-shaped pattern was observed, depended on the sample. The *d* values for ER296, ER323 and ER353 were 90, 100, and 110 μm, respectively, which is in accordance with the SEM results. In general, crazing can be identified by USAXS as a typical cross-shaped pattern of two streaks, where one is positioned along the stretching direction and the other perpendicular.[13,39] Also, the formation of microvoids provides an ellipse pattern, whose major axis is located along the direction normal to the stretch.[29,30] However, no such patterns were observed for ER296, ER323 and ER353 even at a *d* of 10 μm. This is in accordance with a previous report in which no crazing took place for a highly cross-linked epoxy resin.[22] Thus, it seems reasonable to claim that for ER296, ER323 and ER353, cracking occurred prior to crazing and/or the microvoid formation upon the application of strain.

3.3. Local deformation of network.

To discuss a possible origin of the difference in the crack length, and thereby the toughness, among the three resins, the local deformation of the network near the notch tip was examined by microbeam WAXS measurements. Figure 6 shows 2D WAXS patterns for ER296, ER323 and ER353 without any stretching ($\varepsilon = 0$) and the corresponding one-dimensional profiles. All samples yielded a circular WAXS pattern with homogeneous intensity distribution. In the WAXS profiles, a broad peak was observed at a scattering vector (q) of 12 nm^{-1}, corresponding to a domain spacing (d-spacing) of 0.54 nm. In general, a scattering contrast in WAXS arises from differences in the electron density. Since the electron density for the hydroxy-tertiary amine linkage, that formed via the reaction between epoxy and amino groups, is relatively higher than that for other aliphatic moieties, the d-spacing should reflect the distance between them.[40] Postulating that the linkage is in the cross-linking point of the network, the d-spacing obtained here would reflect the network mesh size. In fact, the d-spacing was the same for all three samples, which possessed the same ν and ρ, as shown in Table 1.

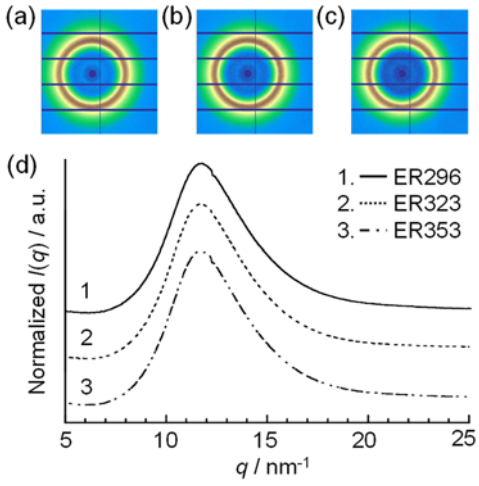

Figure 6. Two-dimensional WAXS patterns for (a) ER296, (b) ER323 and (c) ER353 without any stretching. (d) WAXS profiles obtained by circular averaging each pattern shown in panels (a)−(c).

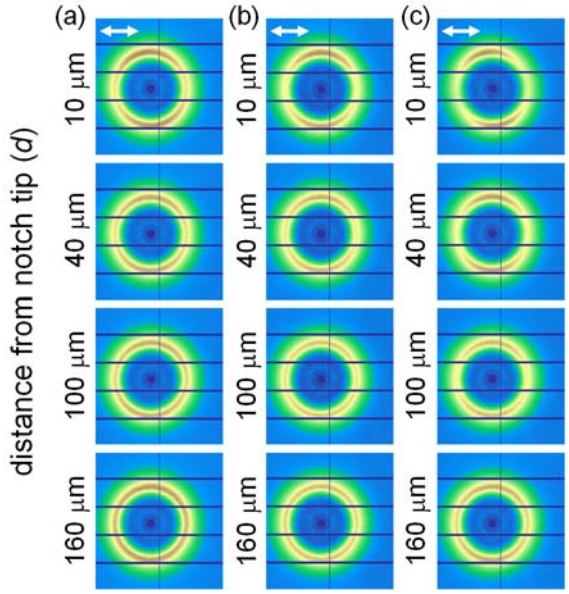

Figure 7. Two-dimensional WAXS patterns at various *d*s for (a) ER296, (b) ER323 and (c) ER353 at ε of 0.03. The white double arrows in the top row denote the stretching direction.

Each specimen was stretched at ε of 0.03, a strain at which cracks did not yet generate from the notch tip. Also, there was no scattering due to crazes and/or microvoids, as revealed by the USAXS measurements (see Figure S4 in the Supporting Information). Figure 7 shows representative 2D WAXS patterns as a function of *d* for the stretched ER296, ER323 and ER353. At a *d* of 10 μm for ER296, the scattering was strongly observed along the meridian direction,

which corresponded to the direction normal to the stretching. Such an anisotropic pattern indicates that segments align along the direction parallel to the stretching due to the deformation of the network mesh.[41,42] The anisotropy of the pattern seems to decrease with increasing *d* up to 160 μm, meaning that the deformation of the network became less marked the farther away from the notch. Here, it should be noted that the *d* at which the anisotropy in the pattern disappeared was dependent on the sample, namely the pre-curing temperature.

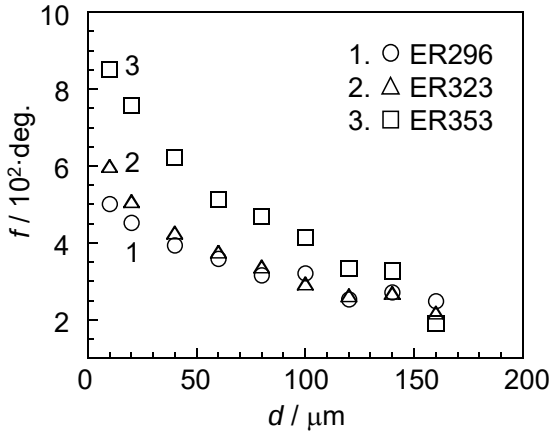

Figure 8. Values of *f* obtained from the azimuthal intensity profile as a function of *d* for ER296, ER323 and ER353 at ε of 0.03.

To confirm such a trend, the azimuthal intensity profile at a *q* of 12 nm^{-1} was examined (see Figure S5 in the Supporting Information). The extent of the anisotropy, and thereby the network deformation, was then quantified as an apparent Herman's orientation function (*f*).[42,43] The *f* value ranges from −0.5 to 1 for chains which are aligned perfectly perpendicular and parallel to the stretching direction, respectively, while it reverts to be zero for an isotropic system.[43] Figure 8 shows the *f* value as a function of *d* for ER296, ER323 and ER353 stretched at ε of 0.03. The *f* value decreased with increasing *d* from near the notch tip and this was the case for all epoxy resins. However, the *f* value was higher in the order of ER353, ER323 and ER296 at a given *d*, especially in close proximity to the notch tip. This makes it clear that the network deformation became more remarkable as the extent of the heterogeneity increased. Generally, the stress applied by stretching is concentrated in less-dense regions in which a large

deformation occurs.[27,42,44] This scenario can explain the large deformation observed for ER353, which possesses a heterogeneous network composed of denser and less-dense cross-linked regions. Taking into account that the generation and propagation of cracks were initiated by the deformation, the difference in the crack length, and thereby the toughness, depending on the heterogeneity can be reasonably understood.

4. CONCLUSIONS

We studied the mechanical properties and fracture behavior including the crack propagation for epoxy resins obtained via different curing processes. Epoxy resins used in this study were obtained by pre-curing a mixture of HDGEBA and CBMA at three different temperatures, 296 K, 323 K and 353 K, then middle-curing. They were then post-cured for various times to unify their cross-linking and mass densities. The resultant network is supposed to be more heterogeneous as pre-curing temperature increases. The yield stress and fracture energy, and thereby the toughness, were lower as the pre-curing temperature increased. *In-situ* SEM observation for the stretch-induced deformation of the epoxy resins with a notch revealed that the crack propagation generated from the notch tip was more marked with increasing pre-curing temperatures. Based on microbeam USAXS measurements, no crazes and/or microvoids were found around the crack of the stretched epoxy resins. To obtain information on the network deformation, microbeam WAXS measurements were taken at different positions of the epoxy resins stretched at a smaller strain, where the crack was not yet generated. In the case of the epoxy resin pre-cured at higher temperatures, the network structure was more deformed, and the deformation reached a position farther away from the notch. Such deformation behavior can be associated with the difference in the crack length and the toughness of the three epoxy resins. The findings obtained in this study will be useful for understanding and controlling the toughness of epoxy resins.

ACKNOWLEDGEMENTS

We are grateful for support from the JST-Mirai Program (JPMJMI18A2) (K.T.) and the JSPS KAKENHI for Scientific Research (B) (no. JP20H02790) (K.T.), (no. JP22H01795) (A.S.). The SEM experiments were performed at the Analysis Center in Fukuoka Industry-Academia Symphonicity. The synchrotron radiation facilities experiments were performed at BL05XU in the SPring-8.

SUPPORTING INFORMATION

Supporting Information is available free of charge on the ACS Publications website.

Sample preparation, X-ray transmittance measurement, Scanning electron microscopic (SEM) observation, Wide-angle X-ray scattering (WAXS) measurement

REFERENCES

(1) Pruksawan, S.; Samitsu, S.; Yokoyama, H.; Naito, M. Homogeneously Dispersed Polyrotaxane in Epoxy Adhesive and Its Improvement in the Fracture Toughness. *Macromolecules* **2019**, *52*, 2464−2475.

(2) Hanafusa, A.; Ando, S.; Ozawa, S.; Ito, M.; Hasegawa, R.; Mayumi, K.; Ito, K. Viscoelastic Relaxation Attributed to the Molecular Dynamics of Polyrotaxane Confined in an Epoxy Resin Network. *Polym. J*. **2020,** *52*, 1211−1221.

(3) Shundo, A.; Yamamoto, S.; Tanaka, K. Network Formation and Physical Properties of Epoxy Resins for Future Practical Applications. *JACS Au* **2022**, *2*, 1522–1542. adhesion

(4) Huang, Y.; Deng, L.; Ju, P.; Huang, L.; Qian, H.; Zhang, D.; Li, X.; Terryn, H. A.; Mol, J. M. C. Triple-Action Self-Healing Protective Coatings Based on Shape Memory Polymers Containing Dual- Function Microspheres. *ACS Appl. Mater. Interfaces* **2018**, *10*, 23369−23379.

(5) Xu, X.; Shi, S.; Tang, Y.; Wang, G.; Zhou, M.; Zhao, G.; Zhou, X.; Lin, S.; Meng, F. Growth

of NiAl-Layered Double Hydroxide on Graphene Toward Excellent Anticorrosive Microwave Absorption Application. *Adv. Sci*. **2021**, 2002658.

(6) Yang, S. C.; Kwak, S.-Y.; Jin, J. H.; Kim, J.-S.; Choi, Y.; Paik, K.-W.; Bae, B.-S. Thermally Resistant UV-curable Epoxy–siloxane Hybrid Materials for Light Emitting Diode (LED) Encapsulation. *J. Mater. Chem*. **2012**, *22*, 8874–8880.

(7) Aoki, M.; Shundo, A.; Okamoto, K.; Ganbe, T.; Tanaka, K. Segregation of an Amine Component in a Model Epoxy Resin at a Copper Interface. *Polym. J*. **2019**, *51*, 359−363.

(8) Aoki, R.; Yamaguchi, A.; Hashimoto, T.; Urushisaki, M.; Sakaguchi, T.; Kawabe, K.; Kondo, K.; Iyo, H. Preparation of Carbon Fibers Coated with Epoxy Sizing Agents Containing Degradable Acetal Linkages and Synthesis of Carbon Fiber-reinforced Plastics (CFRPs) for Chemical Recycling. *Polym. J*. **2019**, *51*, 909–920.

(9) Yang, K.; Guan, J.; Numata, K.; Wu, C. G.; Wu, S. J.; Shao, Z. Z.; Ritchie, R. O. Integrating Tough Antheraea Pernyi Silk and Strong Carbon Fibres for Impact-critical Structural Composites. *Nat. Commun.*, **2019**, *10*, 3786.

(10) Bellenger, V.; Verdu, J.; Morel, E. Effect of Structure on Glass Transition Temperature of Amine Crosslinked Epoxies. *J. Polym. Sci., Part B: Polym. Phys*. **1987**, *25*, 1219−1234.

(11) Shundo, A.; Aoki, M.; Yamamoto, S.; Tanaka, K. Cross-Linking Effect on Segmental Dynamics of Well-Defined Epoxy Resins. *Macromolecules* **2021**, *54*, 5950−5956.

(12) Shundo, A.; Aoki, M.; Yamamoto, S.; Tanaka, K. Effect of Cross-Linking Density on Horizontal and Vertical Shift Factors in Linear Viscoelastic Functions of Epoxy Resins. *Macromolecules* **2021**, *56,* 9618−9624.

(13) Jansen, B. J. P.; Rastogi, S.; Meijer, H. E. H.; Lemstra, P. J. Rubber-Modified Glassy Amorphous Polymers Prepared via Chemically Induced Phase Separation. 2. Mode of Microscopic Deformation Studied by in-Situ Small-Angle X-ray Scattering during Tensile Deformation. *Macromolecules* **2001**, *34*, 4007–4018.

(14) Maier, A. G.; Wallner, G.; Lang, R. W.; Fratzl, P. Structural Changes during Plastic Deformation at Crack Tips in PVDF Films: A Scanning X-ray Scattering Study. *Macromolecules* **2005**, *38*, 6099−6105.

(15) Zafeiropoulos, N. E.; Davies, R. J.; Roth, S. V.; Burghammer, M.; Schneider, K.; Riekel, C.; Stamm, M. Microfocus X-Ray Scattering Scanning Microscopy for Polymer

Applications. *Macromol. Rapid Commun*. **2005**, *26*, 1547–1551. polymer, various events

(16) Lei, C.; Xu, R.; Tian, Z.; Huang, H.; Xie, J.; Zhu, X. Stretching-Induced Uniform Micropores Formation: An in Situ SAXS/WAXS Study. *Macromolecules* **2018**, *51*, 3433–3442.

(17) Yan, Q.; Zhang, W.; Wu, T.; Lin, Y.; Wang, D.; Meng, L.; Chen, W.; Li, L. Understanding the Brittle-ductile Transition of Glass Polymer on Mesoscopic Scale by In-situ Small Angle X-ray Scattering. *Polymer* **2020**, *209*, 122985-1–10.

(18) Liu, C.; Feng, S.; Zhu, Z.; Chen, Q.; Noh, K.; Kotaki, M.; Sue, H.-J. Manipulation of Fracture Behavior of Poly(methyl methacrylate) Nanocomposites by Interfacial Design of a Metal–Organic-Framework Nanoparticle Toughener. *Langmuir* **2020**, *36*, 11938–11947.

(19) Wang, P. P.; Maeda, R.; Aoki, M.; Kubozono, T.; Yoshihara, D.; Shundo, A.; Kobayashi, T.; Yamamoto, S.; Tanaka, K.; Yamada, S. In Situ Transmission Electron Microscopy Observation of the Deformation and Fracture Processes of an Epoxy/Silica Nanocomposite. *Soft Matter* **2022,** *18*, 1149−1153.

(20) Morgan, R. J.; Mones, E. T.; Steele, W. J. Tensile Deformation and Failure Processes of Amine-cured Epoxies. *Polymer* **1982**, *23*, 295−305.

(21) Narisawa, I.; Murayama, T.; Ogawa, H. Internal Fracture of Notched Epoxy Resins. *Polymer* **1982**, *23*, 291−294.

(22) Sue, H.-J. Study of Rubber-modified Brittle Epoxy Systems. Part II: Toughening Mechanisms under Mode-I Fracture. *Polym. Eng. Sci*. **1991**, *31*, 275−288.

(23) Sue, H.-J. Craze-like Damage in a Core-shell Ruber-modified Epoxy System. *J. Mater. Sci.* **1992**, *27*, 3098−3107.

(24) J. P. Bell, Mechanical Properties of a Glassy Epoxide Polymer: Effect of Molecular Weight between Crosslinks. *J. Appl. Polym. Sci.* **1970**, *14*, 1901−1906.

(25) K. Cho, D. Lee, C. E. Park and W. Huh, Effect of Molecular Weight between Crosslinks on Fracture Behaviour of Diallylterephthalate Resins. *Polymer* **1996**, *37*, 813−817.

(26) Aoki, M.; Shundo, A.; Kuwahara, R.; Yamamoto, S.; Tanaka, K. Mesoscopic Heterogeneity in the Curing Process of an Epoxy-amine System. *Macromolecules* **2019**, *52*, 2075−2082.

(27) Aoki, M.; Shundo, A.; Yamamoto, S.; Tanaka, K. Effect of A Heterogeneous Network on Glass Transition Dynamics and Solvent Crack Behavior of Epoxy Resins. *Soft Matter* **2020**,

16, 7470−7478.

(28) Nguyen, H. K.; Aoki, M.; Liang, X.; Yamamoto, S.; Tanaka, K.; Nakajima, K. Local Mechanical Properties of Heterogeneous Nanostructures Developed in a Cured Epoxy Network: Implications for Innovative Adhesion Technology. *ACS Appl. Nano Mater.* **2021**, *4*, 12188–12196.

(29) Zhang, H.; Scholz, A. K.; de Crevoisier, J.; Vion-Loisel, F.; Besnard, G.; Hexemer, A.; Brown, H. R.; Kramer, E. J.; Creton, C. Nanocavitation in Carbon Black Filled Styrene–Butadiene Rubber under Tension Detected by Real Time Small Angle X-ray Scattering. *Macromolecules* **2012**, *45*, 1529–1543.

(30) Zhang, H.; Scholz, A. K.; de Crevoisier, J.; Berghezan, D.; Narayanan, T.; Kramer, E. J.; Creton, C. Nanocavitation around a Crack Tip in a Soft Nanocomposite: A Scanning Microbeam Small Angle X-ray Scattering Study. *J. Polym. Sci., B: Polym. Phys.* **2015**, *53,* 422–429.

(31) Scetta, G.; Euchler, E.; Ju, J.; Selles, N.; Heuillet, P.; Ciccotti, M.; Creton, C. Self-Organization at the Crack Tip of Fatigue-Resistant Thermoplastic Polyurethane Elastomers. *Macromolecules* **2021**, *54*, 8726–8737.

(32) Xue, W.; Champ, S.; Huglin, M. B. Network and Swelling Parameters of Chemically Crosslinked Thermoreversible Hydrogels. *Polymer* **2001**, *42*, 3665−3669.

(33) Feger, C.; MacKnight, W. F. Properties of Partially Cured Networks. 2. The Glass Transition. *Macromolecules* **1985**, *18*, 280–284.

(34) Yamamoto, S.; Ida, R.; Aoki, M.; Kuwahara, R.; Shundo, A.; Tanaka, K. Formation Mechanism of a Heterogeneous Network in Epoxy Resins. *Macromolecules* submitted (ma-2023-00411v.R1).

(35) Xie, Q.; Liang, S.; Liu, B.; Fu, K.; Zhan, Z.; Lu, L.; Yang, X.; Lü, F.; Huang, Z. Structure, Microparameters and Properties of Crosslinked DGEBA/MTHPA: A Molecular Dynamics Simulation. *AIP Adv*. **2018**, *8*, 075332-1–14.

(36) Kinloch, A. J.; Williams, J. G. Crack Blunting Mechanisms in Polymers. *J. Mater. Sci*. **1980**, *15*, 987–996.

(37) Volynskii, A. L.; Bazhenov, S.; Lebedeva, O. V.; Bakeev, N. F. Mechanical Buckling Instability of Thin Coatings Deposited on Soft Polymer Substrates. *J. Mater. Sci.* **2000**, *35*,

547–554.

(38) Salmons, G. J.; Singh, M. A.; Bardouille, T.; Foran, W. A.; Capel, M. S. Small-Angle X-ray Scattering Study of Craze Formation and Dynamics in Thermoplastics. *Macromolecules* **1999**, *32*, 1264–1270.

(39) Zafeiropoulos, N. E.; Davies, R. J.; Schneider, K.; Burghammer, M.; Riekel, C.; Stamm M. The Relationship between Craze Structure and Molecular Weight in Polystyrene as Revealed by μSAXS Experiments. *Macromol. Rapid Commun.* **2006**, *27,* 1689–1694.

(40) Dušek, K.; Pleštil, J.; Lednický F.; Luňák, S. Are Cured Epoxy Resins Inhomogeneous? *Polymer* **1978**, *19*, 393–397.

(41) Nishi, K.; Shibayama, M. Probe-SAXS on Hydrogels under Elongation. *Soft Matter* **2016**, *12*, 5334–5339.

(42) Matsumoto, Y.; Shundo, A.; Hayashi, H.; Tsuruzoe, N.; Tanaka, K. Effect of the Heterogeneous Structure on Mechanical Properties for a Nanocellulose-Reinforced Polymer Composite. *Macromolecules* **2019**, *52*, 8266−8274.

(43) Stein, R. S. The X-Ray Diffraction, Birefringence, and Infrared Dichroism of Stretched Polyethylene. II. Generalized Uniaxial Crystal Orientation. *J. Polym. Sci*. **1958**, *31*, 327–334.

(44) S. Yamini and R. J. Young, The Mechanical Properties of Epoxy Resins. *J. Mater. Sci*. **1980**, *15*, 1823–1831.